Proton radiography of dynamic electric and magnetic fields in laser-produced high-energy-density plasmas[a)]

C. K. Li,[1,b)] F. H. Séguin,[1] J. A. Frenje,[1] M. Manuel,[1] D. Casey,[1] N. Sinenian,[1] R. D. Petrasso,[1] P. A. Amendt,[2] O. L. Landen,[2] J. R. Rygg,[2] R. P. J. Town,[2] R. Betti,[3,4] J. Delettrez,[3] J. P. Knauer,[3] F. Marshall,[3] D. D. Meyerhofer,[3,4] T. C. Sangster,[3] D. Shvarts,[3,5] V. A. Smalyuk,[3] J. M. Soures,[3] C. A. Back,[6] J. D. Kilkenny,[6] and A. Nikroo[6]
[1]*Plasma Science and Fusion Center, Massachusetts Institute of Technology, Cambridge, Massachusetts 02139, USA*
[2]*Lawrence Livermore National Laboratory, Livermore, California 94550, USA*
[3]*Laboratory for Laser Energetics, University of Rochester, Rochester, New York 14623, USA*
[4]*Department of Mechanical Engineering, Physics and Astronomy, University of Rochester, Rochester, New York 14623, USA*
[5]*NRCN, Negev and Ben Gurion University of the Negev, Beer-Sheva 84015, Israel*
[6]*General Atomics, San Diego, California 92186, USA*

(Received 4 December 2008; accepted 11 February 2009; published online 24 March 2009)

Time-gated, monoenergetic-proton radiography provides unique measurements of the electric (E) and magnetic (B) fields produced in laser-foil interactions and during the implosion of inertial-confinement-fusion capsules. These experiments resulted in the first observations of several new and important features: (1) observations of the generation, decay dynamics, and instabilities of megagauss B fields in laser-driven planar plastic foils, (2) the observation of radial E fields inside an imploding capsule, which are initially directed inward, reverse direction during deceleration, and are likely related to the evolution of the electron pressure gradient, and (3) the observation of many radial filaments with complex electromagnetic field striations in the expanding coronal plasmas surrounding the capsule. The physics behind and implications of such observed fields are discussed. © *2009 American Institute of Physics*. [DOI: 10.1063/1.3096781]

I. INTRODUCTION

The generation, evolution, interaction, and dissipation of self-generated electric (E) and magnetic (B) fields by interactions of laser light with matter[1] are processes that are of fundamental interest in high-energy-density (HED) physics (pressures >1 Mbar).[2] Many processes contribute to field generation and evolution; their relative importance depends on interaction parameters.[1,3–8] For long-pulse, low-intensity laser light (a regime in which the other sources are relatively unimportant), as illustrated in Fig. 1, the dominant source for B field generation is noncollinear electron density and temperature gradients ($\nabla n_e \times \nabla T_e$).[1,3–8] For circular laser spots, the B fields have a toroidal configuration with scale length comparable to the spot size. In the regime with low Z and high temperature, where resistivity is low, B-field growth is linear in time and is balanced by convective losses (or field transport) [$\nabla \times (\boldsymbol{v} \times \mathbf{B})$, where $\boldsymbol{v}$ is the plasma fluid velocity, i.e., the B field is "frozen in"[1,3–8]]. When the laser is off and the cooling plasma becomes more resistive, field diffusion (or field dissipation) dominates convective transport [$\nabla \times (D_m \nabla \times \mathbf{B})$, where D_m is the magnetic diffusion coefficient[1,3–8]]. Under these circumstances, B field generation and evolution are

$$\frac{\partial \boldsymbol{B}}{\partial t} \approx \nabla \times (\boldsymbol{v} \times \boldsymbol{B}) - \frac{1}{en_e} \nabla n_e \times \nabla T_e - \nabla \times (D_m \nabla \times \boldsymbol{B}). \tag{1}$$

The dominant source for E fields is the electron pressure gradient ($\nabla P_e / n_e$), a consequence of force balance in a single fluid force equation (where electron inertia is neglected),[1,3,4]

$$0 \approx \boldsymbol{E} + \frac{1}{en_e} \nabla P_e. \tag{2}$$

These fields have important implications for several practical problems. In inertial-confinement fusion (ICF),[9–11] B fields generated inside a hohlraum by laser illumination can reduce heat flow, since cross-field thermal conductivity is modified by a factor of $(1+\omega_{ce}^2 \tau^2)^{-1}$, where ω_{ce} is the electron gyrofrequency and τ is the collision time.[1,3,4] The generation of E fields may significantly modify the plasma distribution and enhance the thick-target bremsstrahlung. The effects of these fields are the altered distributions of electron temperature and density, which lead to significantly enhanced laser-plasma instabilities, radiation nonuniformity, and background emission.[10,11]

We developed the method of monoenergetic, charged-particle radiography[6–8,12] to study E and B field generations. The experiments are performed at the OMEGA laser facility.[13] Topics studied include generation, time evolution and instabilities in laser-plasma-generated B fields, reconnection of megagauss (MG) magnetic fields in high-β plasmas, self-generated E and B fields in direct-drive ICF implosions,

[a)]Paper BI1 5, Bull. Am. Phys. Soc. **53**, 20 (2008).
[b)]Invited speaker. Electronic mail: li@psfc.mit.edu.

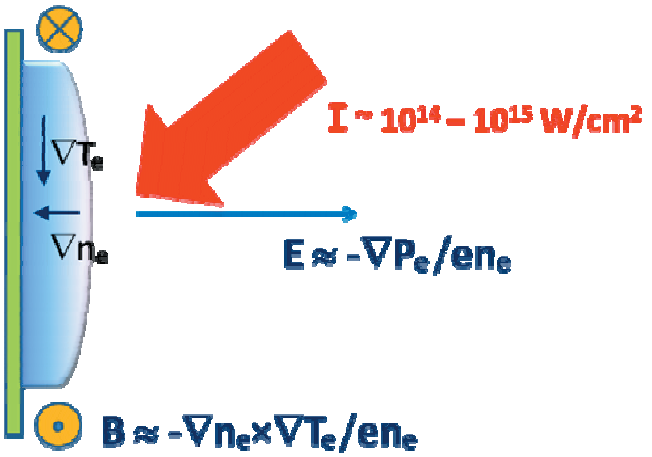

FIG. 1. (Color) Schematic of the generation of self-generated *E* and *B* fields by laser-matter interactions, described by the Faraday equation [Eq. (1)] combined with a simplified version of the generalized Ohm's law (Refs. 1 and 3–8).

B fields associated with Rayleigh–Taylor instabilities in laser-driven foils, and dynamic *E* and *B* fields in laser-driven hohlraums. This work resulted in several important observations.[6–8,12,14,15]

Section II briefly describes the technology of proton radiography and the experiments. The experimental results and discussions are presented in Sec. III. The important findings and results are summarized in Sec. IV.

II. PROTON RADIOGRAPHY OF FIELDS GENERATED BY LASER-PLASMA INTERACTIONS

A. A monoenergetic proton backlighter

To quantitatively probe laser-plasma interactions and particularly resultant *E* and *B* fields, an imaging technology that combines a monoenergetic-particle backlighter with a matched detection system has been developed.[12,16,17] This approach has distinct advantages over radiography with broadband proton sources (such as intense-laser-induced sources).[18] The monoenergetic particles are nuclear fusion products resulting from D^3He-filled, exploding-pusher implosions.[19] 14.7 MeV protons, 3 MeV protons, and 3.6 MeV alphas are generated from the nuclear reactions, as follows:

$$D + {}^3He \rightarrow \alpha(3.6\ \text{MeV}) + p(14.7\ \text{MeV}), \tag{3}$$

$$D + D \rightarrow T(1\ \text{MeV}) + p(3\ \text{MeV}). \tag{4}$$

Backlighter implosions are typically driven with 20 or fewer OMEGA laser beams (wavelength of 0.351 μm) (Ref. 13) in a 8–10 kJ, 1 ns square pulse; no phase plates or smoothing by spectral dispersion[20,21] are used. The capsule diameter is about 440 μm to minimize the proton source size for improved spatial resolution. A comprehensive set of diagnostics are used to characterize the implosion, including both proton-emission and x-ray-emission images for studying the size of the imploded capsule and its burn region, spectrometers for measuring the proton energy spectrum[12,16,17] and a proton temporal diagnostic to measure the bang time and

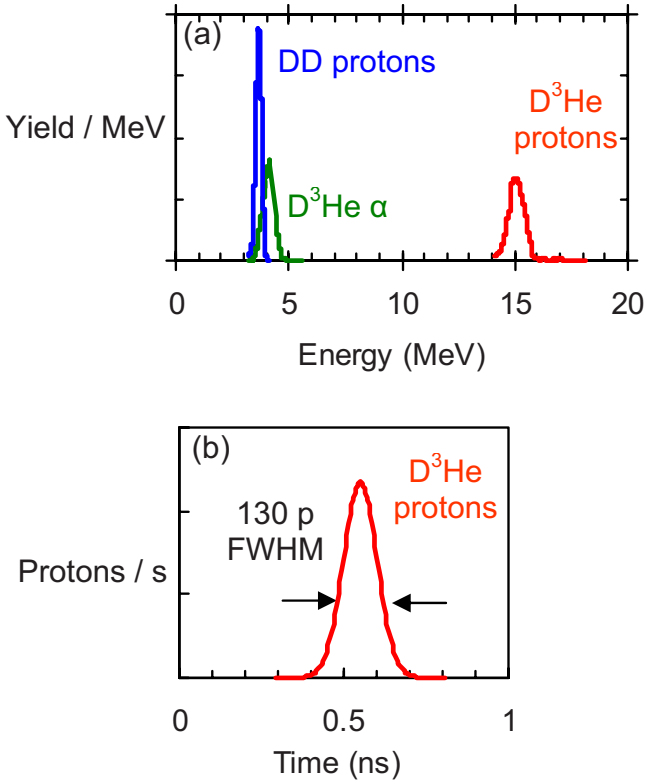

FIG. 2. (Color online) (a) Spectra and (b) time history of charged fusion products from an exploding pusher target at OMEGA containing D^3He fuel. Note that the particle energies are slightly upshifted from their birth energies, due to the charging of the capsule during the 1 ns square laser pulse illumination (Ref. 12).

burn duration.[22] The fusion products are monoenergetic [Fig. 2(a)] and produced during a ~130 ps time interval [Fig. 2(b)]. The size of the emitting region is measured[12] to be about 40 μm full width at half maximum. The relative timing of the primary interaction and the backlighter implosion is adjusted so that the radiographic image records the condition of the laser-induced plasma at different times providing coarse time resolution.

B. Proton radiography of laser-produced high-energy-density plasmas

The backlighters are used in the configuration shown in Fig. 3. The isotropic nature of the source permits two different subjects to be backlit at the same time, at different angles

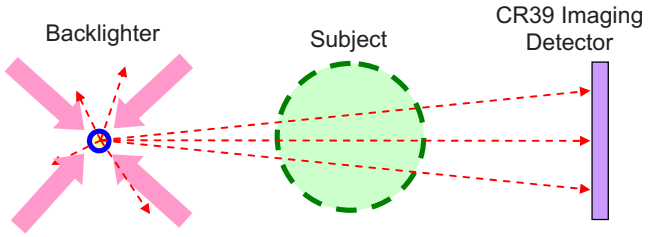

FIG. 3. (Color online) Basic configuration of the monoenergetic charged particle radiography setup. Sample subjects are shown in Fig. 4. In some cases, a single backlighter is used to image two subjects located at 90° or 180° relative to the backlighter; each subject has its own detector. Typical system dimensions are 1 cm from backlighter to subject and 30 cm from backlighter to detector.

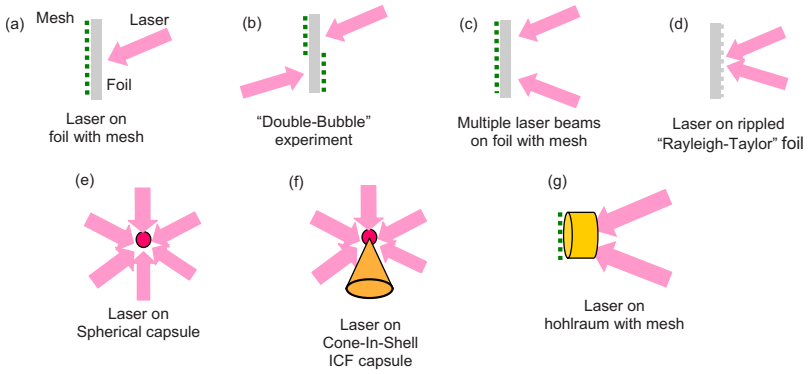

FIG. 4. (Color online) Some of the subjects used in radiography experiments, with the configuration shown in Fig. 3 and the imaging particles incident from the left. The images that result from subjects (a)–(d), with the particles placed normally in relation to the foil, are referred to as "face-on," because they show structure in the plane of the foil. Images of these subjects are also recorded with the hohlraum oriented parallel to the imaging particles, showing the "end-on" structure. In subjects (a)–(c) and (g), the dots (green) are mesh grids.

relative to the backlighter. This maximizes the amount of data that can be accumulated during a given number of shots. The proton-flux images are recorded with CR-39 detectors (1500 μm thick). The tracks in CR-39 are increasingly smaller as proton energy increases above ~1 MeV, which allows us to determine the incident proton energy from the track size. Detection efficiency is 100%. After the detectors are etched in NaOH, the location of incidence of each proton is identified.

Some of the radiographed subjects are shown in Fig. 4 and will be discussed in the following subsections. The monoenergetic character of the particles used for imaging allows two kinds of measurements to be simultaneously made. The energy loss of the particle while passing through the subject allows the areal density of the subject to be inferred.[23,24] Deflections of the trajectories of the particles by B or E fields can be measured and used to quantitatively determine the field strengths. In some experiments, the measurement of particle deflection is made easier by the insertion of a metal mesh between the backlighter and the subject, as indicated in Figs. 4(a)–4(c) and 4(g); the mesh divides the protons into beamlets whose individual positions can be measured with high accuracy at the detector.

Figure 5 shows how a single plasma bubble, formed by the interaction of a laser beam with a plastic (CH) foil, is surrounded by a toroidal magnetic field. This field deflects individual proton beamlets to form a well defined image, the individual positions of which can be compared on the detector with the positions they would have had in the absence of the magnetic field (for example, the region outside the plasma bubble).[6–8] The identification of the field as B rather than E is demonstrated unambiguously[6,12,25] from an image obtained with the subject shown in Fig. 4(b).[25]

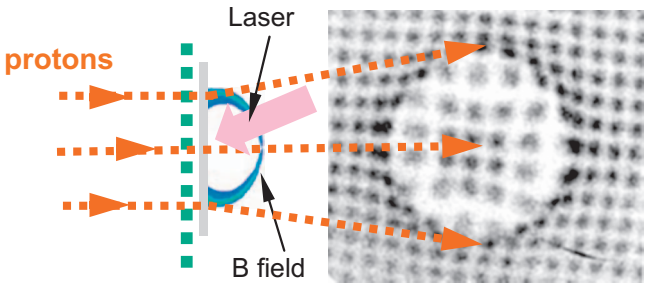

FIG. 5. (Color) Illustration of a laser-plasma interaction on a CH foil, together with a measured radiography image formed by 15 MeV protons divided into beamlets by a metal mesh (the darker areas indicate more protons) (Ref. 6). LASNEX+LSP simulations (Refs. 26–29) indicate that face-on radiography will be sensitive only to the B field, while side-on radiography will be sensitive only to the E field. This allows E and B fields to be measured separately.

III. DATA AND DISCUSSIONS

A. The generation, time evolution, and instabilities of B fields in laser-driven CH foils

Proton radiography was used to measure the dynamics and evolution of megagauss laser-plasma-generated magnetic field structures, as shown in Fig. 6. The monoenergetic character of the proton source, together with the well-characterized imaging detectors and geometry, makes quantitative analysis of the images possible. The typical field strength is estimated to be $\sim 10^6$ gauss (~1 MG).[6–8] The images show that while the 1 ns 10^{14} W/cm^2 laser beam is on, the field structure expands in tandem with a hemispherical plasma bubble, maintaining two-dimensional (2D) cylindrical symmetry. When the laser turns off, the bubble continues to expand as the field decays, however the outer field structure becomes distinctly asymmetric, indicating instability. Localized asymmetry growth in the bubble interior indicates another kind of instability.[7,30] Figure 7 shows the time evolution of the maximum value of $|\int \mathbf{B}\times d\ell|$. The force on the protons is proportional to $|\mathbf{B}\times d\ell|$, where $d\ell$ is the differential path length along the proton trajectory within the field region. It is plausible that the bubble asymmetry is

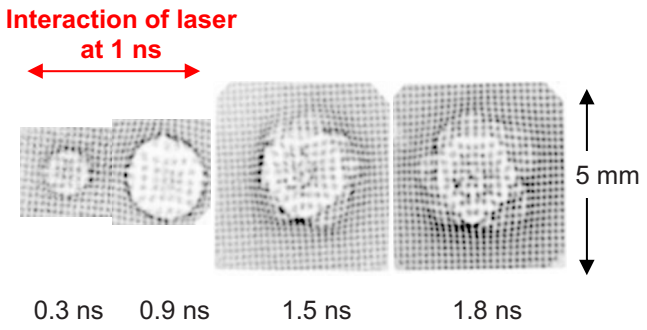

FIG. 6. (Color online) D^{3}He proton radiographs showing the evolution of B fields in a plasma/field bubble formed by the interaction of a laser beam with a CH foil, as described in the text and Ref. 7. The arrangement of the foil with respect to the imaging system is shown in Figs. 3 and 4(a).

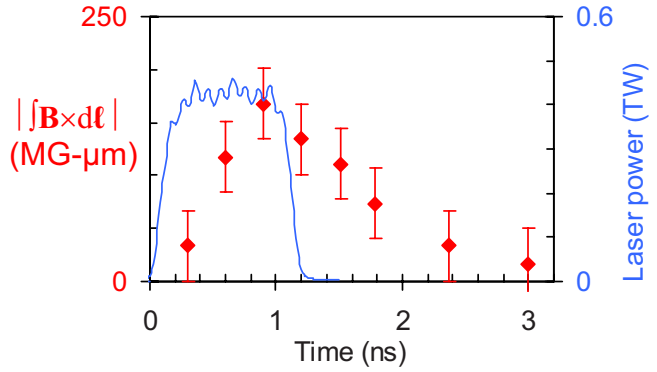

FIG. 7. (Color online) Measured time evolution of the maximum $|\int \mathbf{B}\times d\ell|$, as described in Ref. 7. In this case, the blue curve is the time history of the laser intensity.

caused by pressure-driven, resistive magnetohydrodynamic (MHD) instabilities. Pure fluid instabilities such as the Widnall type[31] might be visible while the laser is on (when B fields do not have much impact on the plasma flow but are frozen in); there is no evidence for this instability occurring.[7]

B. Magnetic reconnection in laser-generated plasmas

The interaction and reconnection of magnetic fields in plasmas are important fundamental processes[32] with implications for a wide range of basic science, including astrophysics,[33] space physics,[34] and laboratory physics.[35,36] In HED plasmas (pressures >1 Mbar),[2] the generation, evolution, and reconnection of B fields due to laser-plasma interactions take place in an extreme physical regime. High plasma densities ($>10^{20}$ cm^{-3}), high temperatures (~ 1 keV), intense B fields (~ 1 MG), and high ratios of thermal pressure to magnetic pressure ($\beta \gg 1$) distinguish this from the tenuous plasmas of the order of 10^{14} cm^{-3} or lower, which are the more traditional venues of reconnection experiments.[33,35] Radiography experiments described in Ref. 8 involved the first direct observation of field reconnection in the HED regime, where plasma flow was dominated by hydrodynamics and was not strongly affected by fields, even though MG fields were present. The setup was as shown in Figs. 3 and 4(c), with two laser beams on a foil. Figure 8 shows where the bubbles interacted and reconnection occurred by 0.67 ns. The images were used to deduce maps of the B field at the foil and the location of each beamlet can be compared with the location it would have had without B fields (beamlets on the image edges define the grid of "undeflected" locations). Quantitative field maps derived from the radiographs directly reveal changes in the magnetic topology due to reconnection in a HED plasma ($n_e \sim 10^{20}$–10^{22} cm^{-3}, $T_e \sim 1$ keV).

These observations provide the first measurements and mapping of the change in field topology associated with reconnection in a high-β, HED plasma. The 2D Sweet–Parker (SP) model[37,38] does not explain the reconnecting dynamics in this case. The experimental reconnection time scale can be estimated as $\tau_{R,E} \sim 0.2$ ns by dividing the apparent width of the field layer at the surface of the bubble in Fig. 8(c) by twice the bubble expansion velocity ($v \sim 5\times 10^7$ cm s^{-1}). In contrast, the SP reconnection time is $\tau_{R,\mathrm{SP}}=(\tau_D\tau_A)^{1/2} \sim 5$ ns, where $\tau_D=0.5L_\perp^2 D_m^{-1} \sim 30$ ns is the B-field diffusion time, $\tau_A=L_\perp v_A^{-1} \sim 1$ ns is the Alfvén transit time, and $v_A \sim 5\times 10^6$ cm s^{-1} (taking $n_i \sim 1\times 10^{20}$ cm^{-3} and inferring from earlier results[6,7] that $B \sim 0.5$ MG for a proton path length $L_\perp \sim 200$ μm). Though there are uncertainties in the estimates of these parameters, the comparison suggests that the reconnection illustrated in Fig. 8 is dominated by plasma hydrodynamics and noncollisional (nondissipative) processes, rather than resistivity. This dominance is connected with the fact that the plasma expansion velocity is faster than the Alfvén velocity. Unlike all previous reconnection experiments,[32–35] the ones described here have a reconnection time shorter than the characteristic Alfvén transit time.[8]

C. Self-generated *E* and *B* fields in direct-drive ICF implosions

Figure 9 shows radiographs taken at different times during implosions of cone-in shell capsules for fast ignition[39] [Fig. 9(a)] and direct-drive spherical implosions[40] [Fig. 9(b)], using the setup of Fig. 3, with subjects oriented as shown in Figs. 4(f) and 4(e), respectively. The capsules are ~ 0.9 mm in diameter and the field of view is much larger.[14,15]

The images reveal several unexpected features due to electromagnetic fields in and around the imploding capsules. In the two images of Fig. 9(a), the region outside the capsule shell is uniform at 0 ns, but full of filaments at 1.5 ns. The deflections of imaging protons necessary to generate this filamentation cannot be explained due to scattering in filamented matter, which would require much more material than is present in the corona. The filamentation must be due to fields and is qualitatively repeatable in different experiments, as seen in the 1.5 ns image of Fig. 9(b). The precise nature and source of the fields responsible for these filaments is under study. As magnetic fields, the filamentation can be shown, from the scale and amplitude of the features, to have a characteristic magnitude of 0.6 MG.[14] The 0.5 ns image in

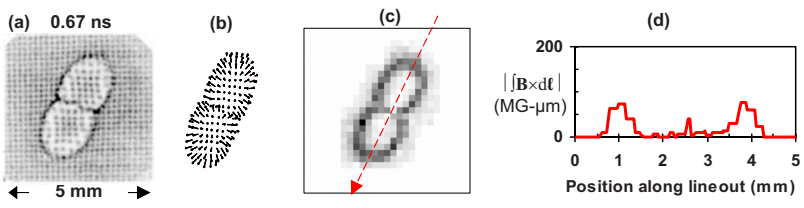

FIG. 8. (Color online) Radiographs (a) generated when two laser beams were incident on a CH foil, showing how magnetic reconnection results in diminished field energy where two plasma bubbles surrounded by magnetic fields collide. (b) shows displacement vectors ξ of the beamlets. Arrays of displacement amplitudes are shown as images in (c); each pixel represents one beamlet, with a value proportional to displacement. The lineouts of (c) (along the red arrow) provide quantitative measurement of $|\int \mathbf{B}\times d\ell|$ at the foil location (d).

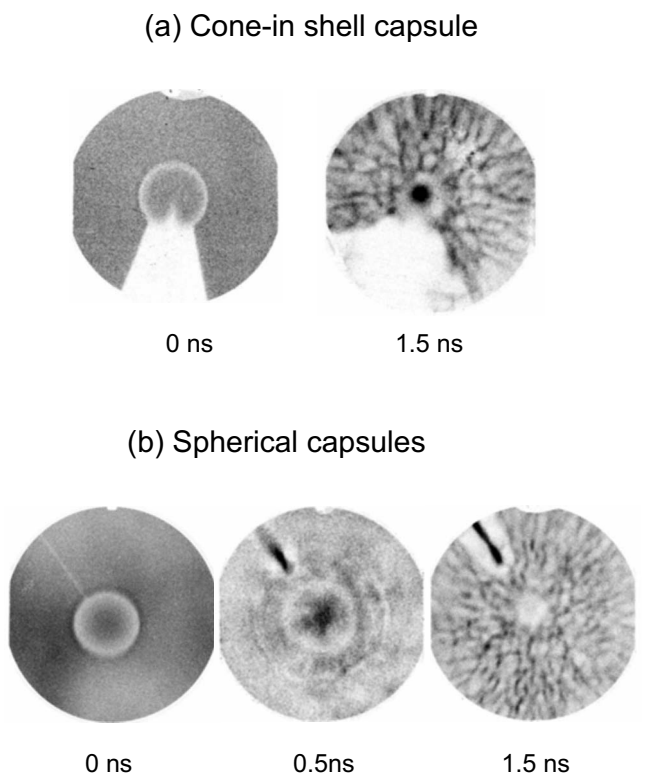

FIG. 9. Proton fluence distributions in radiographs of (a) a 430-μm-radius spherical plastic capsule with attached Au cone, before and during implosion (Ref. 14) and (b) spherical capsules before and during implosion (Ref. 15). In all cases, the 1-ns-long laser drive began at 0 ns. The plastic shells were 24 μm thick in (a) and 20 μm thick in (b). The linear feature in the upper left corner of each image of a spherical capsule is the mounting stalk.

Fig. 9(b) shows that the field structure at earlier times has a different character, since the features outside the capsule have a quasispherical structure. The time evolution of these fields and their transitions from one type to another will be discussed elsewhere. In the following part of this section, we are going to demonstrate the presence of an E field.

The experiments show the existence of a radial E field inside the imploding capsules. The fluence image in Fig. 10 at 0.8 ns shows a concentration of protons in the center. Monte Carlo simulations have shown that the size of this peak cannot be explained by the scattering of imaging protons by the CH shell.[15] It appears to be due to an inward directed radial E field. The images show that the centrally peaked fluence turns into a central fluence deficit at later times ($>$1.4 ns), indicating that the E field has reversed direction. In both cases the estimated field amplitude has a magnitude of $\sim 10^9$ V/m. Figure 11 shows that the experiment-inferred E field magnitude at different times compares well with the field calculated from the pressure gradients predicted by the one-dimensional hydrodynamic code LILAC.[41] This field is probably a consequence of the evolution of the electron pressure gradient [Eq. (2)].

IV. CONCLUSION

In summary, we conducted time-gated, monoenergetic-proton radiography of self-generated electric and magnetic fields associated with laser-foil interactions and imploded ICF capsules. These experiments resulted in the observations

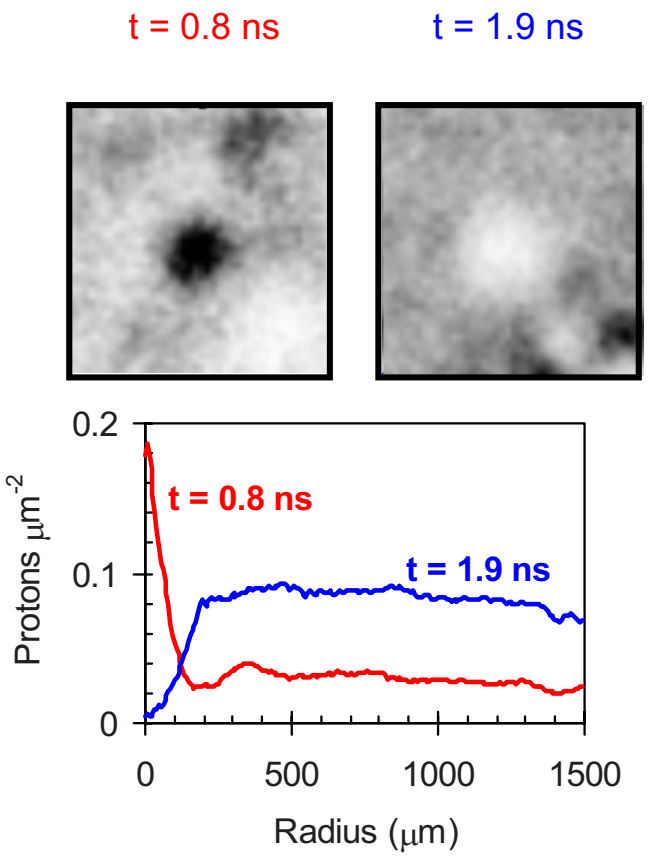

FIG. 10. (Color online) Radial profiles of the proton fluence images measured at t=0.8 and 1.9 ns. Comparatively, a fluence peak occurs in the image centers during the early stages of implosion, indicating a "focusing" of imaging protons there, while in contrast, the fluence is extremely low or defocused at the image centers at later times. Note that the different level ($\times\sim 2$) of the proton fluence outside the capsules ($r > \sim 200$ μm) is due to the variations from the backlighter proton yields.

of several new and important features: (1) the observations of the generation, decay dynamics, instabilities, and reconnection of megagauss B fields in laser-driven planar plastic foils, (2) the observation of radial electric fields inside the

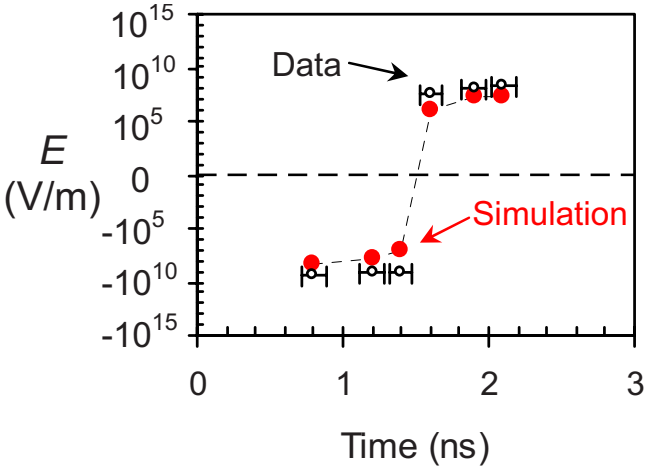

FIG. 11. (Color online) Radial E fields estimated from experimental measurements (open circles) and from LILAC simulations (solid circles) vs implosion times. Horizontal error bars represent uncertainties in backlighter burn time. The differences between simulation and data may result from effects of proton scattering.

imploding capsule that are initially directed inward, reversing direction near the onset of deceleration, and which are likely related to the evolution of the electron pressure gradient, and (3) the observation of many radial filaments with complex electromagnetic field striations. The physics behind and implications of such observed fields have been briefly discussed.

ACKNOWLEDGMENTS

The work was performed at the LLE National Laser User's Facility (NLUF) and was supported in part by U.S. DOE (Grant Nos. DE-FG52-07NA28059 and DE-FG52-06N826203), LLNL (Grant No. B543881), LLE (Grant No. 414090-G), the Fusion Science Center at University of Rochester (Grant No. 412761-G), and GA (Grant No. DE-AC52-06NA27279).

[1] M. G. Haines, Phys. Rev. Lett. **78**, 254 (1997).
[2] R. P. Drake, *High-Energy-Density Physics* (Springer, New York, 2006), pp. 5–8.
[3] L. Spitzer, *Physics of Fully Ionized Gases* (Interscience, New York, 1962), Chap. 2.
[4] S. I. Braginskii, *Review of Plasma Physics* (Consultant Bureau, New York, 1965), pp. 262–276.
[5] M. Borghesi, A. J. Mackinnon, A. R. Bell, R. Gaillard, and O. Willi, Phys. Rev. Lett. **81**, 112 (1998).
[6] C. K. Li, F. H. Seguin, J. A. Frenje, J. R. Rygg, R. D. Petrasso, R. P. J. Town, P. A. Amendt, S. P. Hatchett, O. L. Landen, A. J. Mackinnon, P. K. Patel, M. Tabak, V. A. Smalyuk, T. C. Sangster, and J. P. Knauer, Phys. Rev. Lett. **97**, 135003 (2006).
[7] C. K. Li, F. H. Seguin, J. A. Frenje, J. R. Rygg, R. D. Petrasso, R. P. J. Town, P. A. Amendt, S. P. Hatchett, O. L. Landen, A. J. Mackinnon, P. K. Patel, M. Tabak, J. P. Knauer, T. C. Sangster, and V. A. Smalyuk, Phys. Rev. Lett. **99**, 015001 (2007).
[8] C. K. Li, F. H. Seguin, J. A. Frenje, J. R. Rygg, R. D. Petrasso, R. P. J. Town, O. L. Landen, J. P. Knauer, and V. A. Smalyuk, Phys. Rev. Lett. **99**, 055001 (2007).
[9] J. Nuckolls, L. Wood, A. Thiessen, and G. Zimmerman, Nature (London) **239**, 139 (1972).
[10] J. D. Lindl, *Inertial Confinement Fusion* (Springer-Verlag, New York, 1999).
[11] S. Atzeni and J. Meyer-Ter-Vehn, *The Physics of Inertial Confinement Fusion* (Claredon, Oxford, 2004).
[12] C. K. Li, F. H. Seguin, J. A. Frenje, J. R. Rygg, R. D. Petrasso, R. P. J. Town, P. A. Amendt, S. P. Hatchett, O. L. Landen, A. J. Mackinnon, P. K. Patel, M. Tabak, V. A. Smalyuk, T. C. Sangster, J. P. Knauer, and C. Stoeckl, Rev. Sci. Instrum. **77**, 10E725 (2006).
[13] J. M. Soures, R. L. McCrory, C. P. Verdon, A. Babushkin, R. E. Bahr, T. R. Boehly, R. Boni, D. K. Bradley, D. L. Brown, R. S. Craxton, J. A. Delettrez, W. R. Donaldson, R. Epstein, P. A. Jaanimagi, S. D. Jacobs, K. Kearney, R. L. Keck, J. H. Kelly, T. J. Kessler, R. L. Kremens, J. P. Knauer, S. A. Kumpan, S. A. Letzring, D. J. Lonobile, S. J. Loucks, L. D. Lund, F. J. Marshall, P. W. McKenty, D. D. Meyerhofer, S. F. B. Morse, A. Okishev, S. Papernov, G. Pien, W. Seka, R. Short, M. J. Shoup III, M. Skeldon, S. Skupsky, A. W. Schmid, D. J. Smith, S. Swales, M. Wittman, and B. Yaakobi, Phys. Plasmas **3**, 2108 (1996).
[14] J. R. Rygg, F. H. Séguin, C. K. Li, J. A. Frenje, M. J.-E. Manuel, R. D. Petrasso, R. Betti, A. Delettrez, O. V. Gotchev, J. P. Knauer, D. D. Meyerhofer, F. J. Marshall, C. Stoeckl, and W. Theobald, Science **319**, 1223 (2008).
[15] C. K. Li, F. H. Seguin, J. R. Rygg, J. A. Frenje, M. Manuel, R. D. Petrasso, R. Betti, J. Delettrez, J. P. Knauer, F. Marshall, D. D. Meyerhofer, D. Shvarts, V. A. Smalyuk, C. Stoeckl, O. L. Landen, R. P. J. Town, C. A. Back, and J. D. Kilkenny, Phys. Rev. Lett. **100**, 225001 (2008).
[16] F. H. Séguin, J. A. Frenje, C. K. Li, D. G. Hicks, S. Kurebayashi, J. R. Rygg, B.-E. Schwartz, R. D. Petrasso, S. Roberts, J. M. Soures, D. D. Meyerhofer, T. C. Sangster, J. P. Knauer, C. Sorce, V. Yu. Glebov, C. Stoeckl, T. W. Phillips, R. J. Leeper, K. Fletcher, and S. Padalin, Rev. Sci. Instrum. **74**, 975 (2003).
[17] F. H. Séguin, J. L. DeCiantis, J. A. Frenje, C. K. Li, J. R. Rygg, C. D. Chen, R. D. Petrasso, J. A. Delettrez, S. P. Regan, V. A. Smalyuk, V. Yu. Glebov, J. P. Knauer, F. J. Marshall, D. D. Meyerhofer, S. Roberts, T. C. Sangster, C. Stoeckl, K. Mikaelian, H. S. Park, H. F. Robey, and R. E. Tipton, Phys. Plasmas **13**, 082704 (2006).
[18] A. J. Mackinnon, P. K. Patel, R. P. Town, M. J. Edwards, T. Phillips, S. C. Lerner, D. W. Price, D. Hicks, M. H. Key, S. Hatchett, S. C. Wilks, M. Borghesi, L. Romagnani, S. Kar, T. Toncian, G. Pretzler, and O. Willi, Rev. Sci. Instrum. **75**, 3531 (2004).
[19] M. D. Rosen and J. H. Nuckolls, Phys. Fluids **22**, 1393 (1979).
[20] S. Skupsky and R. S. Craxton, Phys. Plasmas **6**, 2157 (1999).
[21] D. D. Meyerhofer, J. A. Delettrez, R. Epstein, V. Yu. Glebov, V. N. Goncharov, R. L. Keck, R. L. McCrory, P. W. McKenty, F. J. Marshall, P. B. Radha, S. P. Regan, S. Roberts, W. Seka, S. Skupsky, V. A. Smalyuk, C. Sorce, C. Stoeckl, J. M. Soures, R. P. J. Town, B. Yaakobi, J. D. Zuegel, J. Frenje, C. K. Li, R. D. Petrasso, F. H. Se'guin, K. Fletcher, S. Padalino, C. Freeman, N. Izumi, R. Lerche, T. W. Phillips, and T. C. Sangster, Phys. Plasmas **8**, 2251 (2001).
[22] J. A. Frenje, C. K. Li, F. H. Se'guin, J. Deciantis, S. Kurebayashi, J. R. Rygg, R. D. Petrasso, J. Delettrez, V. Yu. Glebov, C. Stoeckl, F. J. Marshall, D. D. Meyerhofer, T. C. Sangster, V. A. Smalyuk, and J. M. Soures, Phys. Plasmas **11**, 2798 (2004).
[23] C. K. Li and R. D. Petrasso, Phys. Rev. Lett. **70**, 3059 (1993).
[24] C. K. Li and R. D. Petrasso, Phys. Rev. Lett. **70**, 3063 (1993).
[25] R. D. Petrasso, C. K. Li, F. H. Seguin, J. R. Rygg, J. A. Frenje, M. Manuel, R. Betti, J. P. Knauer, D. D. Meyerhofer, D. Shvarts, V. A. Smalyuk, O. L. Landen, and R. P. J. Town, Bull. Am. Phys. Soc. **52**, 97 (2007).
[26] G. B. Zimmerman and W. L. Kruer, Comments Plasma Phys. Controlled Fusion **2**, 51 (1975).
[27] P. D. Nielsen and G. B. Zimmerman, "Treatment of q-directed magnetic fields in LASNEX," Lawrence Livermore National Laboratory Report No. UCRL-53123, 1981.
[28] D. R. Welch, D. V. Rose, B. V. Oliver, and R. E. Clark, Nucl. Instrum. Methods Phys. Res. A **464**, 134 (2001).
[29] R. P. J. Town, W. E. Alley, M. J. Edwards, J. H. Hammer, L. J. Suter, M. Tabak, G. B. Zimmerman, D. H. Froula, S. H. Glenzer, G. Gregori, A. J. Mackinnon, P. K. Patel, M. G. Hains, C. K. Li, and R. D. Petrasso, Bull. Am. Phys. Soc. **50**, 26 (2005).
[30] M. G. Haines, Phys. Rev. Lett. **47**, 917 (1981).
[31] S. E. Widnall, D. B. Bliss, and C. Tsai, J. Fluid Mech. **66**, 35 (1974).
[32] D. Biskamp, *Magnetic Reconnection in Plasmas* (Cambridge University Press, Cambridge, 2000), pp. 118–125.
[33] S. Masuda, T. Kosugi, H. Hara, S. Tsuneta, and Y. Ogawara, Nature (London) **371**, 495 (1994).
[34] T. D. Phan, J. T. Gosling, M. S. Davis, R. M. Skoug, M. Aieroset, R. P. Lin, R. P. Lepping, D. J. McComas, C. W. Smith, H. Reme, and A. Balogh, Nature (London) **439**, 175 (2006).
[35] J. B. Taylor, Rev. Mod. Phys. **58**, 741 (1986).
[36] M. A. Yates, D. B. van Hulsteyn, H. Rutkowski, G. Kyrala, and J. U. Brackbill, Phys. Rev. Lett. **49**, 1702 (1982).
[37] P. A. Sweet, Nuovo Cimento, Suppl. **8**, 188 (1958).
[38] E. N. Parker, Astrophys. J., Suppl. **8**, 177 (1963).
[39] M. Tabak, J. Hammer, M. E. Glinsky, W. L. Kruer, S. C. Wilks, J. Woodworth, E. M. Campbell, and M. D. Perry, Phys. Plasmas **1**, 1626 (1994).
[40] R. L. McCrory, D. D. Meyerhofer, R. Betti, R. S. Craxton, J. A. Delettrez, D. H. Edgell, V. Yu. Glebov, V. N. Goncharov, D. R. Harding, D. W. Jacobs-Perkins, J. P. Knauer, F. J. Marshall, P. W. McKenty, P. B. Radha, S. P. Regan, T. C. Sangster, W. Seka, R. W. Short, S. Skupsky, V. A. Smalyuk, J. M. Soures, C. Stoeckl, B. Yaakobi, D. Shvarts, J. A. Frenje, C. K. Li, R. D. Petrasso, and F. H. Séguin, Phys. Plasmas **15**, 055503 (2008).
[41] J. Delettrez, R. Epstein, M. C. Richardson, P. A. Jaanimagi, and B. L. Henke, Phys. Rev. A **36**, 3926 (1987).